

Thermodynamic stability of mixed Pb:Sn methyl-ammonium halide perovskites

Ksenia Korshunova,¹ Lars Winterfeld,¹ Wichard J.D. Beenken,¹ and Erich Runge¹

¹*Institut für Physik and Institut für Mikro- und Nanotechnologie,
Technische Universität Ilmenau, 98684 Ilmenau, Germany*

(Dated: June 20, 2016)

Using density functional theory, we investigate systematically mixed $MA(Pb : Sn)X_3$ perovskites, where MA is $CH_3NH_3^+$, and X is Cl , Br or I . Ab initio calculations of the orthorhombic, tetragonal and cubic perovskite phases show that the substitution of lead by tin has a much weaker influence on both structure and cohesive energies than the substitution of the halogen. The thermodynamic stability of the $MA(Pb : Sn)X_3$ mixtures at finite, non-zero temperatures is studied within the Regular Solution Model. We predict that it will be possible to create $MA(Pb : Sn)I_3$ mixtures at any temperature. Our results imply that mixing is unlikely for the low-temperature phase of bromide and chloride compounds, where instead local clusters are more likely to form. We further predict that in the high-temperature cubic phase, Pb and Sn compounds will mix for both $MA(Pb : Sn)Br_3$ and $MA(Pb : Sn)Cl_3$ due to the entropy contribution to the Helmholtz free energy.

This is the peer reviewed version of the following article: Phys. Status Solidi B, 253: 1907–1915, which has been published in final form at DOI: 10.1002/pssb.201600136. This article may be used for non-commercial purposes in accordance with Wiley Terms and Conditions for Self-Archiving.

I. INTRODUCTION

Solar cells based on hybrid organic-inorganic perovskites as light absorbers have recently received an enormous interest due to their potential to be manufactured much cheaper than monocrystalline silicon cells using, e.g., wet chemistry and spin coating [1–4]. In this context, the term “hybrid organic-inorganic perovskites” refers to a broad class of metal halides that can be described with the general chemical formula ABX_3 , where A is an organic cation, such as (but not limited to) methylammonium ($CH_3NH_3^+$, MA)[5–7], ethylammonium ($CH_3CH_2NH_3^+$, EA)[8, 9], formamidinium ($HC(NH_2)_2^+$, FA)[10–12] or guanidinium ($CH_6N_3^+$, GA)[13, 14], B is a metal cation (usually lead), and X is a halide anion. The metal cations are coordination centers of BX_6 octahedra. We focus on compounds, which build a corner-connected three-dimensional network. The organic cations A are located in the cub-octahedral cavities between the BX_6 octahedra. Therefore, their size is limited to fit the cavity without major distortions of the octahedral network. Since the stability of the organic-inorganic superlattice strongly depends on the size of A , the relatively small MA-cation is one of the most commonly used organic compounds. Lead-based perovskite solar cells with MA as organic cation reach electrical power conversion efficiencies (PCE) of 16% [15–17], and in the most recently published reports the PCE reaches 18% for mesoporous $MAPbI_3$. [18] In the case of $FAPbI_3$ -based solar cells, the achieved maximum PCE is greater than 20%. [19] However, in view of the potential toxicity of lead, substitution of lead with another group 14 metal, e.g., tin, seems desirable. The search for optimized photoelectric properties initiated a lot of experimental and theoretical research on mixed-halide structures, [3, 4, 20–22] or structures with mixed organic cations. [12, 23] The highest reported efficiencies

at the moment are found for combinations of various organohalide perovskites, such as $FAPbI_3$ mixed with $MAPbBr_3$ with the impressive PCE of 20.1%. [24] Much less is known about the effects of incomplete substitution of lead by other metals. The reason is most likely that researchers either prefer to stick with the very successful $MAPbI_3$ [25] or wish to get rid of Pb altogether. [26–28] Only recently, the mixed $MA Sn_x Pb_{1-x} I_3$ was reported to have a spectrally extended absorption compared to the non-mixed lead-halide perovskites, shifting the absorption onset down to the near infrared. [29–31] Furthermore, effective-mass tuning for improved transport properties was suggested for mixed $Pb:Sn$ iodide compounds in the cubic phase. [32] We think that mixtures with respect to the metal component deserves to be studied in more detail. A better understanding of the whole class of hybrid organohalide perovskites may in the end even lead to Pb-free high-performance cells.

In this paper, we provide a systematic *ab-initio* investigation of $MA BX_3$ perovskites, where B is Sn^{2+} , Pb^{2+} or various mixtures thereof, and X is I^- , Br^- or Cl^- . The starting point is the discussion of general structural and energetic properties of the non-mixed structures in three phases (orthorhombic, tetragonal, and cubic, known from $MAPbI_3$ at different temperatures) depending on their chemical composition. We then introduce a variety of mixed Sn-Pb structures, which differ not only by the total Sn:Pb-ratio but also by the arrangement of the metal atoms in the unit cell. Based on the calculated cohesive energies of these mixed compounds, we employ the Regular Solution Model in order to investigate their thermodynamic stability. Details are described in the next section.

II. METHODOLOGY

We used density functional theory (DFT) to calculate the energy for several atomic structures, as described in the first subsection below. However, DFT alone does not account for entropy contributions, which are relevant for finite temperature predictions. Therefore, a thermodynamic model is needed, which is described in the second subsection.

A. Electronic structure and geometry optimization

To optimize crystal structures and calculate binding energies, we performed *ab initio* DFT calculations using the Vienna Ab initio Simulation Package (VASP).[33, 34] Projector-augmented wave (PAW)[35, 36] adapted pseudopotentials were used. For Pb and Sn atoms, the *d* semi-core states were treated explicitly as valence states with an extended version of PAW potentials. The generalized gradient approximation (GGA) parametrized by Perdew-Burke-Ernzerhof (PBE)[37] was employed for the evaluation of the exchange-correlation functional. The Brillouin zone was sampled with Γ -centered *k*-point grids of $5 \times 5 \times 3$, $5 \times 5 \times 3$, and $5 \times 5 \times 5$ for the orthorhombic, tetragonal, and cubic unit cells, respectively. The minimal cutoff energy was set to 500 eV for both the geometry optimization calculations and the self-consistent energy calculations. The convergence threshold for self-consistent-field iteration was set to 10^{-4} eV. As a starting point for the geometry optimization, we used experimentally obtained data from powder X-ray diffraction (PXRD) measurements of *MA PbI₃* carried out by Stoumpos *et al.*[11] for the tetragonal phase, and Baikie *et al.*[5] for the orthorhombic and cubic phases (with additional theoretical results by Giorgi *et al.*).[6]

B. Thermodynamic model

The thermodynamic stability of alloys can often be understood in terms of nearest-neighbor two-particle interactions only, especially if the substitution compounds are chemically similar. To gain some insight into the thermodynamic stability of mixed *Pb:Sn* perovskites, we describe every BX_6 octahedron as one unit placed on a three-dimensional lattice, which interacts only with its $Z = 6$ nearest-neighbor octahedra. Small distance variations in bond length, which occur in structures for orthorhombic and tetragonal phase due to unequal primitive vector lengths can be neglected. To be specific, we start with the cohesive energies E of various mixed structures obtained from the self-consistent DFT calculations and describe them as a linear combination of the binding energies \mathcal{E}_{PbPb} , \mathcal{E}_{PbSn} and \mathcal{E}_{SnSn} between PbX_6 and

SnX_6 octahedra. Thus, we write

$$E = \frac{1}{2} (N_{PbPb} \mathcal{E}_{PbPb} + N_{PbSn} \mathcal{E}_{PbSn} + N_{SnSn} \mathcal{E}_{SnSn}) , \quad (1)$$

where N_{PbPb} , N_{PbSn} , N_{SnSn} denote the number of bonds between the corresponding components and the factor $1/2$ has been added to avoid double-counting of the bonds. A simple bond-counting argument shows that the number of PbX_6 octahedra is $N_{Pb} = N_{PbPb}/6 + N_{PbSn}/12$ and we define the fractions $n_{Pb(Sn)} = N_{Pb(Sn)}/N$ with respect to the total number N of octahedra in the system. Note that $n_{Pb} + n_{Sn} = 1$.

Equation (1) is the starting point for the Regular Solution Model (RSM).[38] Its key quantity is the free energy of mixing $F^M = U^M - TS^M$, which is defined as the difference in the Helmholtz free energy between a non-mixed system ($N_{PbSn} = 0$), and a stochastically intermixed ensemble (each octahedron is filled with *Pb* with probability n_{Pb}). The internal energy of mixing U^M is the stochastic average of the difference in cohesive energy over N octahedra and takes the form

$$U^M(n_{Pb}) = N n_{Pb}(1 - n_{Pb}) 6 \varepsilon .$$

The parameter

$$\varepsilon = \mathcal{E}_{PbSn} - \frac{\mathcal{E}_{PbPb} + \mathcal{E}_{SnSn}}{2} \quad (2)$$

determines whether energy is gained or released during the formation of two heterogeneous $PbX_6 - SnX_6$ bonds by means of breaking homogeneous $PbX_6 - PbX_6$ and $SnX_6 - SnX_6$ bonds. Within the RSM, the entropy of mixing S^M depends solely on the number of possible configurations and thus on n_{Pb} via the following expression:

$$S^M(n_{Pb}) = N k_B [n_{Pb} \ln(n_{Pb}) + (1 - n_{Pb}) \ln(1 - n_{Pb})] , \quad (3)$$

where k_B is the Boltzmann constant.

A mixed state is called *ideal* if $\varepsilon = 0$ and *regular* otherwise. In the case of a regular solution, there are two possible scenarios. If the mixing parameter ε is negative, the heterogeneous bond is always energetically favorable and thus mixing of the components is preferred at any temperature. The more interesting case where the mixing parameter ε is positive, requires a closer examination. In this case, the miscibility of the components depends on the interplay between the internal energy of mixing U^M , which favors the formation of clusters of only one kind of octahedra and thus phase separation, and the temperature-dependent entropic term, $-TS^M$, which favors mixing.

At low temperatures, the U^M term prevails and the system separates into two phases at all ratios n_{Pb} . With increasing temperature, the entropic term causes a change in the shape of the $F^M(n_{Pb})$ curve, which leads to the reduction of the so-called mixing gap. At the *upper critical solution temperature* T_{UCS} , this gap closes and the system experiences no phase separation anymore.

Within the RSM, the value of T_{UCS} can be calculated from the condition $0 = \left. \frac{\partial F^M}{\partial n_{Pb}} \right|_{T=T_{UCS}}$ as:

$$T_{UCS} = \frac{6\varepsilon(2n_{Pb} - 1)}{k_B [\ln(n_{Pb}) - \ln(1 - n_{Pb})]}, \quad (4)$$

with a maximum $T_{UCS} = 3\varepsilon/k_B$ at $n_{Pb} = 0.5$. Experimental deviations from this universal result are observed, e.g., for polymer mixtures, where the building blocks are of different volume and geometry. Such systems are better described by the Flory-Huggins solution model,[39, 40] which is an extension of the RSM.

Note that we do not include the entropic contribution stemming from the different orientations of the organics. This contribution is key for understanding the phase transition between, e.g., the tetragonal and the cubic phase. However, it can be neglected for the question of mixing within one phase, because such entropic terms cancel out in equation (3).

III. GEOMETRY OF OPTIMIZED STRUCTURES

In this section, we analyze the optimized structures of hybrid metal-organic halide perovskites $MA(Pb : Sn)X_3$. First, we discuss the geometry of the *non-mixed* structures containing solely either *Pb* or *Sn*. In particular, we compare the octahedral distortions in the three phases and among different compositions and provide for a possible explanation within the framework of the orbital energy matching model.[41] We then discuss the *mixed* systems, i.e., those with both *Pb* and *Sn* as metal cations. Understanding the geometry of the mixed systems will be the basis for the thermodynamic considerations in section IV.

A. Comparison of non-mixed hybrid perovskites

For all investigated hybrid metal-organic perovskites, the lowest energy configuration forms an orthorhombic Bravais lattice, i.e., the lattice vectors differ in length ($a \neq b \neq c$), but are orthogonal. Concordantly, it is the preferred structure at low temperatures. However, we also investigated the tetragonal ($a = b \neq c$) and cubic ($a = b = c$) phases, which have been observed in experiments at higher temperatures.[42] For the prototypical $MAPbI_3$, the transition temperatures are 162 K (-111°C) and 327 K (54°C). The geometry of all three phases is illustrated for a particular example in Figure 1. Note that in all cases the PbI_3 octahedra are corner-connected, i.e., each *Pb* cation has exactly six *I* anions as nearest neighbors and each *I* anion is connected to two *Pb* cations. In the tetragonal phase, alternating octahedra along the *c* axis are rotated within the *a-b*-plane by an angle of approximately 22.5° . In the orthorhombic phase, the optimal (lowest energy) orientation of the

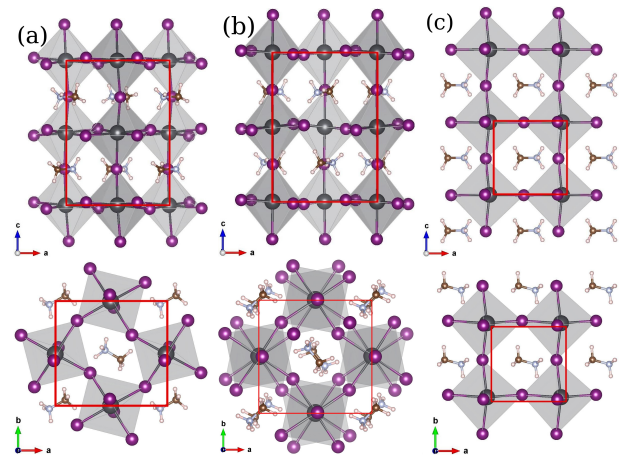


FIG. 1: Comparison of (a) orthorhombic, (b) tetragonal and (c) cubic perovskite phases obtained from structural optimization for the case of $MAPbI_3$. Top row: *a-c*-plane, bottom row: *a-b*-plane.

organics is predetermined by the nearly cuboctahedral cavities between the PbI_6 octahedra and any rotation of the *MA* cations is geometrically hindered. As a consequence, the equilibrium volume of the cubic unit cell of $MAPbI_3$ is 5% larger than the orthorhombic cell. The cubic symmetry allows at least three different equivalent orientations (due to the three dimensions). Consequently, rotation of *MA* is more likely in the cubic phase. We found an upper limit for the rotational barrier for *MA* of approximately 60 meV using minimal-energy-chain-of-states calculations. Even though the finite temperature dynamics of the organics in cubic $MAPbI_3$ is an interesting research topic of its own,[43] in this paper we will only consider the lowest energy configuration in the cubic phase, where all organic groups are aligned parallelly (shown in Figure 1c). Some details of the calculations are worthwhile to be noted explicitly: The unit cells of the orthorhombic and tetragonal phases contain 4 formula units of $MAPbI_3$ each. While the rotation of the octahedra is fixed in the orthorhombic and tetragonal phases, it is necessary to use an even number of primitive cells in the cubic supercell in each space direction to allow for possible alternating rotations of the octahedra. Thus, for the cubic phase, we used a larger supercell of $2 \times 2 \times 2$ primitive cells, thus containing 8 formula units. While the octahedra deform during relaxation (as discussed below), we do not find any alternating rotations of the octahedra in the cubic phase. For the orthorhombic phase, we allowed a full relaxation of both ion positions and lattice vectors (including volume). In the tetragonal and cubic phases, we found the optimal volume by a fit to the Murnaghan equation of state[44], where we preserved the tetragonal symmetry of the unit cell by keeping the *c/a*-ratio at the experimentally obtained value of 1.429 [11].

The structural parameters calculated for both mixed and non-mixed structures are listed in Table I. Already

compound	orthorhombic			tetragonal		cubic
	a[Å]	b[Å]	c[Å]	a[Å]	c[Å]	a[Å]
<i>MAPbI₃</i>	9.18	8.65	12.87	9.06	12.94	6.45
<i>MA_{0.25}Sn_{0.75}PbI₃</i>	9.08	8.66	12.85	9.03	12.90	6.43
<i>MA_{0.5}Sn_{0.5}Pb_{0.5}I₃[c]</i>	9.05	8.64	12.79	9.03	12.90	6.44
<i>MA_{0.5}Sn_{0.5}Pb_{0.5}I₃[d]</i>	9.18	8.58	12.78	9.01	12.87	6.43
<i>MA_{0.5}Sn_{0.5}Pb_{0.5}I₃[l]</i>	9.16	8.63	12.79	9.04	12.91	6.42
<i>MA_{0.75}Sn_{0.25}PbI₃</i>	9.04	8.61	12.73	9.00	12.85	6.41
<i>MA_{0.75}Sn_{0.25}PbI₃</i>	9.02	8.64	12.66	8.84	12.54	6.40
<i>MAPbBr₃</i>	8.74	8.11	12.10	8.54	12.21	6.04
<i>MA_{0.25}Sn_{0.75}PbBr₃</i>	8.64	8.12	12.05	8.52	12.17	6.04
<i>MA_{0.5}Sn_{0.5}Pb_{0.5}Br₃[c]</i>	8.62	8.09	12.06	8.52	12.17	6.04
<i>MA_{0.5}Sn_{0.5}Pb_{0.5}Br₃[d]</i>	8.72	8.09	12.01	8.50	12.14	6.04
<i>MA_{0.5}Sn_{0.5}Pb_{0.5}Br₃[l]</i>	8.65	8.08	12.09	8.52	12.18	6.04
<i>MA_{0.75}Sn_{0.25}PbBr₃</i>	8.67	8.12	12.00	8.49	12.12	6.04
<i>MA_{0.75}Sn_{0.25}PbBr₃</i>	8.91	8.11	12.04	8.34	11.83	6.04
<i>MAPbCl₃</i>	8.47	7.62	11.58	8.23	11.76	5.76
<i>MA_{0.25}Sn_{0.75}PbCl₃</i>	8.35	7.76	11.53	8.21	11.73	5.76
<i>MA_{0.5}Sn_{0.5}Pb_{0.5}Cl₃[c]</i>	8.30	7.69	11.64	8.21	11.73	5.76
<i>MA_{0.5}Sn_{0.5}Pb_{0.5}Cl₃[d]</i>	8.37	7.74	11.50	8.19	11.70	5.76
<i>MA_{0.5}Sn_{0.5}Pb_{0.5}Cl₃[l]</i>	8.43	7.72	11.47	8.21	11.74	5.76
<i>MA_{0.75}Sn_{0.25}PbCl₃</i>	8.45	7.79	11.58	8.18	11.68	5.76
<i>MA_{0.75}Sn_{0.25}PbCl₃</i>	8.74	7.93	11.77	8.04	11.40	5.76

TABLE I: Calculated crystallographic data of mixed *Pb:Sn* hybrid perovskites in the orthorhombic ($a \neq b \neq c$), tetragonal ($a = b \neq c$) and cubic ($a = b = c$) phases. The suffixes [c], [d] and [l] refer to the chain, diagonal and layered structures, respectively (see Figure 3 below). Note that the volume per formula is $V_0 = a^3$ for the cubic cells, but $V_0 = abc/4$ and $V_0 = a^2 c/4$ for the orthorhombic and tetragonal cells, respectively.

for the non-mixed structures, we see that the substitution of the halogen has a much stronger influence on the crystallographic data than the substitution of the metal cation. To give an example, the lattice parameter c in the orthorhombic phase changes only from 12.87 Å for *MAPbI₃* to 12.66 Å for *MA_{0.75}Sn_{0.25}PbI₃*, while already the bromide-containing structure *MAPbBr₃* has a value for $c = 12.10$ Å well below both iodide compounds. The value for c in the chloride structure is even lower. Table I shows that this holds for each of the investigated *MAX₃* structures.

In summary, the volume of the unit cell is the largest in the (high-temperature) cubic phase and the smallest in the (low-temperature) orthorhombic phase and decreases upon increasing electronegativity of the substituted halogen within each phase.

B. Octahedral distortions and tilt angles

While *PbI₆* octahedra keep their regular shape after geometry relaxation, we noticed that they become more deformed in other *BX₆* compositions. In order to quantify this observation and investigate the influence of the halogen, we calculate the mean volume of the irregular octahedra, V_{\boxtimes} , and a ratio ξ describing the deformation

of the *BX₆* octahedra. The latter is defined in terms of the shortest (d_{min}^{B-X}) and the longest (d_{max}^{B-X}) *B-X* bond lengths as

$$\xi := \frac{d_{max}^{B-X}}{d_{min}^{B-X}} - 1. \quad (5)$$

If the octahedron is symmetric and thus all bond lengths are equal, then $\xi = 0$. If the octahedron is deformed or if the central metal atom is displaced off the center, then $\xi > 0$. Furthermore, we calculate two tilt angles, ϕ and θ , corresponding to the in-plane and the axial angles of the *X-B-X* bonds, respectively. A graphical representation of the tilt angles can be found in Figure 2, which also shows the extreme cases of octahedral distortion found in the orthorhombic phase. While the *PbI₃* octahedra (top row) show only minimal distortions and maintain a regular shape, the *SnCl₃* octahedra (bottom row) are highly distorted.

In Table II, we summarize θ , ϕ , ξ and V_{\boxtimes} for all investigated *MAX₃* structures. The tilt angles θ and ϕ strongly depend on whether the system is orthorhombic, tetragonal or cubic, but show smaller variance for different compositions in the same phase. Note that even in the cubic phase, θ and ϕ deviate from 180°, which is already visible in Figure 1(c) and can be attributed to effects like the interaction of the octahedra with the dipole

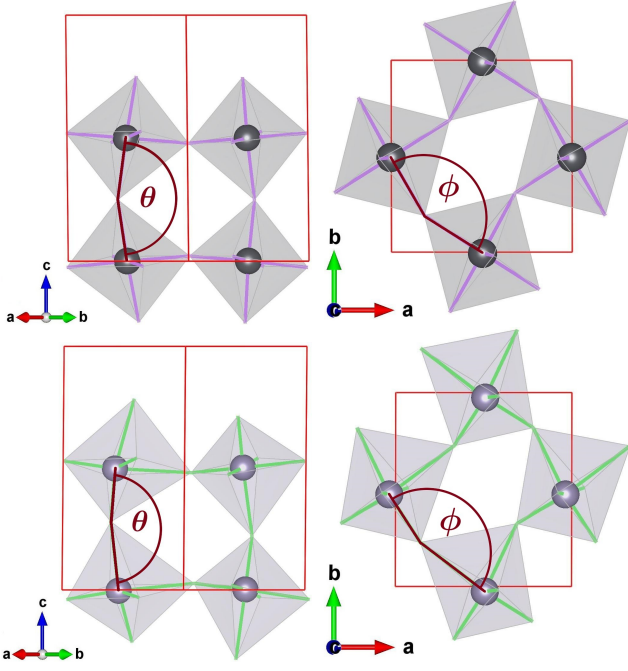


FIG. 2: Tilt angles for octahedral distortions. Top row: $MAPbI_3$. Bottom row: $MASnCl_3$. Note that the Pb ion is positioned approximately at the center of the PbI_3 octahedra, whereas the $SnCl_3$ octahedra are strongly deformed and Sn is placed eccentrically.

moment of the MA cation and the sterically hindered rotation of the octahedra[43, 45, 46].

The mean volume of the octahedra V_{\Box} , on the other hand, shows a strong dependence on the halogen, but depends only weakly on the type of the Bravais lattice. Note that the octahedra always fill between 16.5% (cubic $MAPbI_3$) and 18.2% (orthorhombic $MASnCl_3$) of the unit cell. In the iodide structures, the PbI_6 octahedra have larger V_{\Box} than the SnI_6 octahedra in all phases. Such a general statement can not be made in the case of bromide and chloride containing structures: In the orthorhombic phase, the tin bromide and tin chloride octahedra are larger than their lead counterparts; while in the tetragonal phase, the lead bromide and lead chloride octahedra are larger. Comparing V_{\Box} for the same composition along different phases, we see that V_{\Box} is maximal in the tetragonal phase for Pb -centered octahedra, but minimal for Sn -centered ones.

In all phases, the deformation parameter ξ is much larger for Sn -derived structures than for their Pb counterparts. Among them, $SnCl_3$ (in the low-temperature phases) exhibits the strongest deformations. This can be attributed to the high electronegativity of the ligand and can be explained within the framework of the “orbital energy matching” model.[41] It is based on the Linear Combination of Atomic Orbitals approximation (LCAO). According to this model, the formation of a strong bond between the orbital of the metal cation (tin) and the halogen np orbital occurs when the orbitals are of compatible

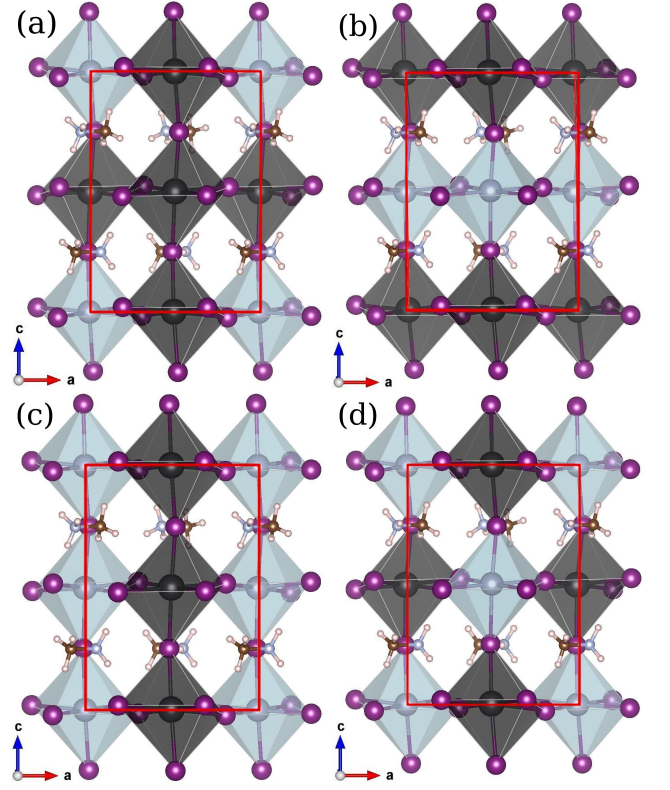


FIG. 3: Mixed orthorhombic $Pb:Sn$ perovskite structures with the following ratios and composition: (a) 3:1, (b) 1:1 and “layer”, (c) 1:1 and “chain”, (d) 1:1 and “diagonal”. Dark octahedra are Pb -centered, light octahedra are Sn -centered.

symmetry and similar energy. To match the energy of a np halogen p -valence orbital, the percentage of $5s$ and $5p$ atomic tin orbitals is changed during the hybridization. For tin iodide structures, the percentage of the p orbital in the bonding hybrid tin orbital is maximal, since the $5p$ orbital of iodine has the highest cohesive energy among the discussed halogens. Because of the orthogonality requirement, the non-bonding hybrid orbital containing the lone pair has mainly s -character and low spatial directionality. With the decreasing cohesive energy of the np orbital of the halogen, the non-bonding hybrid orbital of tin obtains stronger p character, which makes it spatially directed and more stereochemically active. Thus, the octahedral distortions caused by the stereochemically active lone pair on tin increases upon the increase of the electro-negativity of the involved halogen. Apparently, our plane-wave DFT results confirm this simple LCAO-based argument.

C. Properties of mixed $Sn:Pb$ hybrid perovskites

To investigate mixed $Pb:Sn$ hybrid perovskites, we calculated cohesive energies and optimal geometries of five different unit cells as shown in Figure 3. While the geometry will be discussed in this section, results based on

	orthorhombic				tetragonal				cubic			
	$\theta[^\circ]$	$\phi[^\circ]$	$V_{\Box}[\text{\AA}^3]$	ξ	$\theta[^\circ]$	$\phi[^\circ]$	$V_{\Box}[\text{\AA}^3]$	ξ	$\theta[^\circ]$	$\phi[^\circ]$	$V_{\Box}[\text{\AA}^3]$	ξ
<i>MAPbI₃</i>	161	148	42.22	3%	174	157	46.06	2%	172	168	44.17	8%
<i>MA₂SnI₃</i>	164	150	43.93	9%	176	162	41.87	2%	173	167	43.71	16%
<i>MAPbBr₃</i>	159	153	38.28	2%	173	159	38.93	4%	173	168	36.73	7%
<i>MA₂SnBr₃</i>	162	146	38.86	26%	176	163	34.97	9%	172	168	36.73	22%
<i>MAPbCl₃</i>	159	155	33.21	3%	173	165	33.47	6%	172	168	31.91	4%
<i>MA₂SnCl₃</i>	162	143	37.10	42%	173	159	31.23	21%	172	168	31.91	24%

TABLE II: Calculated data for octahedra in different phases and with different compositions. V_{\Box} denotes the mean octahedral volume. For the definition of tilt angles θ and ϕ , see Figure 2. The deformation ratio ξ is defined in equation (5).

the energy value are given in the next section. Figure 3(a) shows a structure with a *Pb:Sn*-ratio of 3:1, corresponding to the formula *MA₂Sn_{0.25}Pb_{0.75}X₃*. Similarly, one can construct a cell with a ratio of 1:3 (not shown), corresponding to the formula *MA₂Sn_{0.75}Pb_{0.25}X₃*. For the 1:1 ratio (*MA₂Sn_{0.5}Pb_{0.5}X₃*), we considered three different structures that we call “layer”, “chain” and “diagonal” as depicted in Figure 3 (b), (c) and (d), respectively. The “chains” are formed by corner-connected octahedra of the same kind along the longest axis (*c*), whereas the “layered” structure consists of alternating layers of *Pb* and *Sn* centered octahedra, perpendicular to the longest axis. This also coincides with the different orientation of the MA relative to the chains and layers, respectively. In the “diagonal” structure, shown in Figure 3(d), all bonds between next nearest octahedra have different metal cations, analogous to a three dimensional checkerboard. The octahedra coordination numbers of all considered structures are listed in Table III.

The structures shown in Figure 3 have been completely relaxed. It is worthwhile to note two details. First, the organic MA molecules change their orientations only slightly and approximately maintain their center position. We conclude that the organic is only weakly influenced by the change of the metal cation. Second, the octahedra of consecutive layers are slightly tilted out of *a*-*b*-plane in opposite directions in all 1:1 structures, which can be seen, e.g., from the positions of the left-most iodide ions in Figure 3.

After relaxing the non-mixed Pb and Sn structures in the cubic phase, we found that the equilibrium lattice constant for chloride structures was $a = 5.763 \text{ \AA}$ for both *MAPbCl₃* and *MA₂SnCl₃*. Likewise for bromide structures, we found $a = 6.040 \text{ \AA}$ for both *MAPbBr₃* and *MA₂SnBr₃* within the accuracy for three decimal digits. Therefore, we did no further volume optimization for the mixed cubic chloride and bromide structures and only relaxed the atomic positions. For the iodide structures, however, we found an equilibrium lattice constant of 6.40 \AA and 6.45 \AA in case of *MA₂SnI₃* and *MAPbI₃*, respectively. Thus, we relaxed all mixed cubic iodide structures with respect to both the volume and the internal degrees of freedom. In all other cases, we performed a full relaxation as described in section III A. The structural results for all phases are summarized in Table I.

Generally, the lattice parameters *a*, *b* and *c* of the mixed *Pb:Sn* structures lie between the non-mixed reference structures. Similar to the non-mixed structures, the halogen have stronger influence on the crystallographic data than the substitution of metal ions: Within each of the three phases (orthorhombic, tetragonal, cubic), all lattice parameters *a*, *b* and *c* of the mixed *Pb:Sn* structures lie in non-overlapping intervals for the iodide, bromide and chloride compounds, respectively. Overall, the cubic phase shows the smallest relative difference in the crystallographic data.

The tilt angles ϕ and θ of all mixed structures tend to take the average of the non-mixed ones for all octahedra. This can be easily explained by the fact that their rotation is sterically hindered by neighboring octahedra. Analyzing the distribution of V_{\Box} and ξ of the octahedra in mixed systems, we find that the individual octahedra maintain their non-mixed characteristics with only small variance. Thus, it is a good approximation to think of the *PbX₆* and *SnX₆* as rigid building blocks of the mixed *Pb:Sn* structures.

compound	N_{PbPb}	N_{PbSn}	N_{SnSn}
<i>MAPbX₃</i>	6	0	0
<i>MA₂Sn_{0.25}Pb_{0.75}X₃</i>	3	3	0
<i>MA₂Sn_{0.5}Pb_{0.5}X₃</i> [c]	1	4	1
<i>MA₂Sn_{0.5}Pb_{0.5}X₃</i> [d]	0	6	0
<i>MA₂Sn_{0.5}Pb_{0.5}X₃</i> [l]	2	2	2
<i>MA₂Sn_{0.75}Pb_{0.25}X₃</i>	0	3	3
<i>MA₂SnX₃</i>	0	0	6

TABLE III: Octahedra coordination numbers N , common to all three phases. The suffixes [c], [d] and [l] correspond to the chain, diagonal and layered structure, respectively (see Figure 3). The mole-fraction x in formula *MA₂Sn_{1-x}Pb_xX₃* can be calculated from $x = N_{PbPb}/6 + N_{PbSn}/12$.

compound	X=I	X=Br	X=Cl
<i>MA PbX₃</i>	-50.9020	-52.7227	-54.3526
<i>MA Sn_{0.25}Pb_{0.75}X₃</i>	-50.8675	-52.6618	-54.2971
<i>MA Sn_{0.5}Pb_{0.5}X₃</i> [c]	-50.8376	-52.6278	-54.2633
<i>MA Sn_{0.5}Pb_{0.5}X₃</i> [d]	-50.8512	-52.6397	-54.2754
<i>MA Sn_{0.5}Pb_{0.5}X₃</i> [l]	-50.8500	-52.6558	-54.2806
<i>MA Sn_{0.75}Pb_{0.25}X₃</i>	-50.8136	-52.6035	-54.2497
<i>MA SnX₃</i>	-50.7635	-52.6062	-54.2714

TABLE IV: Cohesive energies E per formula unit in eV for the *orthorhombic* phase calculated using DFT. The unit cell used for calculation and shown in Figure 3 contains 4 formula units.

compound	X=I	X=Br	X=Cl
<i>MA PbX₃</i>	-50.8766	-52.6578	-54.2931
<i>MA Sn_{0.25}Pb_{0.75}X₃</i>	-50.8457	-52.6239	-54.2643
<i>MA Sn_{0.5}Pb_{0.5}X₃</i> [c]	-50.8197	-52.5998	-54.2370
<i>MA Sn_{0.5}Pb_{0.5}X₃</i> [d]	-50.8300	-52.6010	-54.2295
<i>MA Sn_{0.5}Pb_{0.5}X₃</i> [l]	-50.8348	-52.6107	-54.2553
<i>MA Sn_{0.75}Pb_{0.25}X₃</i>	-50.8002	-52.5748	-54.1986
<i>MA SnX₃</i>	-50.7627	-52.5216	-54.1783

TABLE V: Cohesive energies E per formula unit in eV for the *tetragonal* phase calculated using DFT. The unit cell used for calculation contains 4 formula units.

IV. ENERGY AND THERMODYNAMICS

A. Cohesive energy results

The cohesive energies of all 63 investigated structures obtained from self-consistent DFT calculations are presented in Tables IV-VI. Since the unit cells of compounds in different phases have different symmetry and contain different number of BX_6 octahedra, the total binding energy of each unit cell was normalized to the energy value per formula unit, which contains one BX_6 octahedron and one MA cation. We now analyze the energy values with respect to three parameters: the substituted halogen, the crystal symmetry of each compound, and the Sn:Pb ratio.

compound	X=I	X=Br	X=Cl
<i>MA PbX₃</i>	-50.8627	-52.7020	-54.3528
<i>MA Sn_{0.25}Pb_{0.75}X₃</i>	-50.8637	-52.6696	-54.3129
<i>MA Sn_{0.5}Pb_{0.5}X₃</i> [c]	-50.8446	-52.6416	-54.2804
<i>MA Sn_{0.5}Pb_{0.5}X₃</i> [d]	-50.8398	-52.6340	-54.2660
<i>MA Sn_{0.5}Pb_{0.5}X₃</i> [l]	-50.8395	-52.6344	-54.2717
<i>MA Sn_{0.75}Pb_{0.25}X₃</i>	-50.8215	-52.6066	-54.2423
<i>MA SnX₃</i>	-50.7913	-52.5742	-54.2117

TABLE VI: Cohesive energies E per formula unit in eV for the *cubic* phase calculated using DFT. The unit cell used for calculation contains 8 formula units.

Comparing structures with different halogens, we can see that the cohesive energies of iodide containing structures lie in the range of -50.90 eV and -50.76 eV, whereas the bromide structures lie in the range of -52.72 eV and -52.52 eV, and the chloride structures lie in the range of -54.35 eV and -54.18 eV.

There is no overlap between the energy ranges of structures with different halogens, and the energy shifts within each halogen group are relatively small (~ 0.2 eV) in comparison to those of the structures with different halogens (~ 1.5 eV). Thus, the substitution of a halogen has the biggest influence on the cohesive energy of a structure, and the stability increases with increasing electronegativity of the halogen.

The low-temperature orthorhombic phase of all compounds has the lowest cohesive energy, as expected. However, for all bromide and chloride containing components, not the cubic, but the tetragonal phase with the experimentally obtained c/a -ratio[11] has the highest cohesive energy. Since in our systematic investigation we have used a defined set of phases that have yet been experimentally confirmed only for the *MA PbI₃* compound, this result questions the stability of the bromide and chloride containing structures in this particular tetragonal phase. A possible explanation for this behavior could be octahedra deformations caused by the mechanism discussed in section IIIB. For instance, the strong dependence of the crystal symmetry on the substituted halogen can be shown by the example of non-mixed *MA SnCl₃*, which exhibits a different phase transition process according to PXRD experiments.[5]

With the variation of the *Sn:Pb* ratio, the cohesive energy for each halogen group increases upon the gradual substitution of *Pb* with *Sn*, i.e., the non-mixed lead-containing compounds are the most stable and the tin-containing compounds the least stable among the *Sn:Pb* mixtures. It is worth noticing that the increase of the energy value is not linear with respect to n_{Pb} , which implies a regular solution with $\varepsilon \neq 0$.

One could very naively estimate the cohesive energy of a system based on the number of components of each type as

$$E^0 = N_{Pb} \mu_{Pb} + N_{Sn} \mu_{Sn} \quad (6)$$

with the chemical potentials μ_{Pb} and μ_{Sn} . This formula, however, does not differentiate between different arrangements of the same *Sn : Pb* ratio, because such a simplified model only considers the numbers of atoms N_{Pb} and N_{Sn} . For example, the chain, layer and diagonal arrangements all have 1:1 ratio and would therefore, according to equation (6), yield the same cohesive energy. The Regular Solution Model (RSM, section IIB) based on equation (1), however, explicitly accounts for the number of bonds of each type. Therefore, it allows us to make predictions for different arrangements of BX_6 octahedra. To calculate the binding energies \mathcal{E}_{PbPb} , \mathcal{E}_{SnSn} and \mathcal{E}_{PbSn} in formula (1), we used the non-mixed *MA PbX₃*, *MA SnX₃*, and the diagonal *MA Sn_{0.5}Pb_{0.5}X₃* structures, respectively,

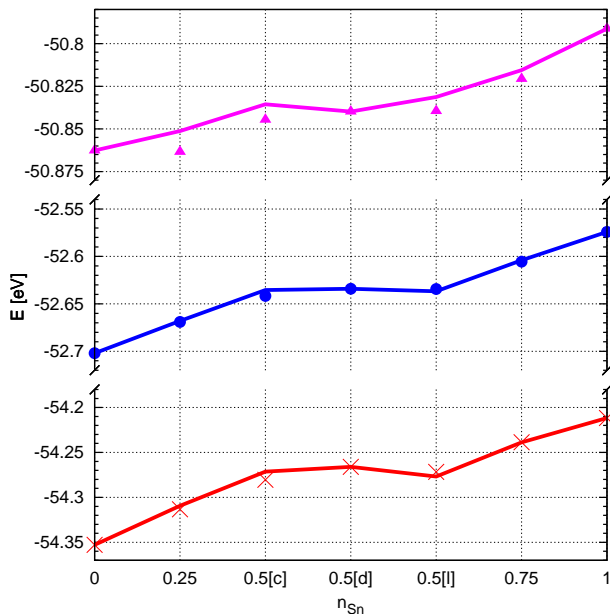


FIG. 4: Comparison of the cohesive energies E per formula unit between the Regular Solution Model (solid lines) and DFT results (symbols) for the cubic phase of iodide $MA(Pb:Sn)I_3$ (top row, \blacktriangle), bromide $MA(Pb:Sn)Br_3$ (middle row, \bullet) and chloride $MA(Pb:Sn)Cl_3$ (bottom row, \times).

since all of them contain only one type of bonds (see Table III). Using equation (2), these three binding energies are condensed into the single parameter, ε . The power of the RSM now lies in the ability to extrapolate to the cohesive energies of structures that were not used to calculate ε . This allows us, for instance, to estimate the cohesive energies of the chain and layer arrangements, as well as the $MA\text{Sn}_{0.25}\text{Pb}_{0.75}\text{X}_3$ and $MA\text{Sn}_{0.75}\text{Pb}_{0.25}\text{X}_3$ structures for each phase and each halogen. We will qualitatively and quantitatively compare these results to the cohesive energies directly obtained from DFT calculations and show that, *a posteriori*, the RSM provides a very good description.

In the orthorhombic phase, equation (1) predicts that the layered structure is the most stable for $\varepsilon > 0$ (bromide and chloride) and the diagonal structure is more stable than chain and layer for $\varepsilon < 0$ (iodide). This agrees with all the cohesive energies obtained from DFT calculations listed in Table IV. In the tetragonal phase, the chain structure is, according to equation (1), more stable than the diagonal reference structure in the case of $\varepsilon > 0$ (chloride), and less stable for $\varepsilon < 0$ (bromide and iodide), again in agreement with our DFT calculations (listed in Table V). In the cubic phase, equation (1) predicts that the layered structure has a lower cohesive energy than the diagonal reference structure for $\varepsilon > 0$ (chloride and bromide) and a higher cohesive energy for $\varepsilon < 0$ (iodide), in agreement with our DFT calculations (Table VI), too.

We will now focus on the high-temperature cubic

phase, which we consider to be most relevant for practical applications. In Figure 4, we plot the obtained values from both DFT and RSM. The root-mean-square deviation between them is only 1.4 meV and 2.2 meV for the bromide and chloride containing structures, respectively. The deviation is higher for the iodide compounds, but since all DFT data points lie on or below the RSM curve in this case, the mixed structures are even more energetically favorable than predicted by the RSM with $\varepsilon = -2.9 \text{ meV} < 0$.

B. Thermodynamic results

The above mentioned parameter ε also plays an important role in estimating the critical mixing temperatures T_{UCS} , which were obtained for each particular phase according to the formula (4). They are summarized in Table VII. To estimate whether the mixed structures containing a particular halogen actually exist, it is necessary to compare the critical mixing temperatures T_{UCS} with the structural phase transition temperatures. Mixing will only occur if the critical temperature T_{UCS} is lower than the transition temperature of that phase. The transition temperatures are known from experiments[42, 47, 48] for non-mixed $MAPbX_3$ for the orthorhombic to tetragonal (tetragonal to cubic) phase transition: they are 162K (328K) for $MAPbI_3$, 146K (236K) for $MAPbBr_3$ and 172K (178K) for $MAPbCl_3$. The different experiments agree within $\pm 2\text{K}$ and the numbers given above are averaged over the values in the cited references. For $MA\text{SnI}_3$, phase transitions are found at 111K (275K)[49]. $MA\text{SnBr}_3$ is known to be in cubic phase at room temperature[50] and calorimetric measurements[51] show a transition at 229K to an experimentally unidentified (possibly tetragonal) phase. Experiments done by Baikie *et al.*[5] show that the non-mixed $MA\text{SnCl}_3$ is in the cubic phase above 463K. Below that temperature, several phases with different Bravais lattices (tricline, monocline and trigonal) are observed. In our calculations, we indeed find a triclinic structure after a full relaxation, however, with only tiny deviations ($< 1^\circ$) from the orthorhombic structure.

For the iodide group, ε has a negative value in all phases, which means that the mixing will occur even at low temperatures.

In the case of the bromide-containing structures, only the tetragonal phases mix at all temperatures. Bromide containing structures in the cubic phase form properly mixed arrangements only above a certain temperature, estimated by us at $T_{UCS} = 54 \text{ K}$. Since T_{UCS} is noticeably below the corresponding phase transition temperatures of 236K and 229K for non-mixed lead and tin compounds, respectively, we conclude that the bromide-containing structure in the cubic phase will always mix. We find that mixing of bromides in the orthorhombic phase is not possible, because above the critical temperature of $T_{UCS} = 288 \text{ K}$, the orthorhombic phase is no

compound	orthorhombic	tetragonal	cubic
$MA(SnPb)I_3$	$\varepsilon = -6.2$ meV	$\varepsilon = -3.4$ meV	$\varepsilon = -2.9$ meV
	-	-	-
$MA(SnPb)Br_3$	$\varepsilon = 8.3$ meV	$\varepsilon = -3.8$ meV	$\varepsilon = 1.6$ meV
	$T_{UCS} = 288$ K	-	$T_{UCS} = 54$ K
$MA(SnPb)Cl_3$	$\varepsilon = 12.2$ meV	$\varepsilon = 2.1$ meV	$\varepsilon = 5.4$ meV
	$T_{UCS} = 425$ K	$T_{UCS} = 72$ K	$T_{UCS} = 187$ K

TABLE VII: Mixing parameter ε , see equation (2), and estimated upper critical solution temperatures T_{UCS} of the mixed $Pb:Sn$ hybrid perovskites. Above T_{UCS} , mixing is favorable due to the entropy contribution. A dash (-) indicates that mixing is preferred at any temperature.

longer stable.

We estimate the critical temperature of the orthorhombic chloride-containing structures to be $T_{UCS} = 425$ K. Since experiments confirmed that the orthorhombic phase is no longer stable at that temperature for the non-mixed chloride compounds, we predict that stochastic mixing in the low temperature phase will not be observed. In the tetragonal and the cubic phase, on the other hand, the mixed structures can be stable, because the critical temperatures of both phases lie below the corresponding phase transition temperatures.

V. SUMMARY

We summarize our main results based on *ab-initio* DFT calculations and extrapolations to non-zero temperatures.

We found that geometric properties of the investigated structures are influenced by two main factors: on the one side chemical composition and on the other side temperature and temperature-driven phase transitions. The unit cell volume increases with temperature, which is linked to the mobility of the organic cation. The deformations of BX_6 octahedra increase with increasing electronegativity of the halogen and are stronger for Sn than for Pb . The crystallographic parameters of the mixed structures fall into the range spanned by the limiting cases of the non-mixed Pb and Sn structures. The shapes of individual BX_6 octahedra slightly change in mixed arrangements in order to preserve the corner-connected structure in the presence of metal ions of different size.

The energy shifts within each halogen group are relatively small in comparison to those of the compounds with different halogens. In particular, there is no overlap

of the cohesive-energy ranges of compounds with different halogens. Thus, the substitution of a halogen has the biggest influence on the cohesive energy of a compound, and the stability increases with increasing electronegativity of the halogen.

With help of the Regular Solution Model (RSM), mixing parameter ε and upper critical solution temperatures T_{UCS} were calculated, which then allowed to estimate the conditions at which the compounds would mix. We predict that it will be possible to create $MA(Pb:Sn)I_3$ mixtures in all three structural phases. Our results also imply that mixing is generally not energetically preferred for the bromide and chloride containing structures, but becomes possible due to the entropy contribution above the calculated upper critical solution temperatures T_{UCS} for tetragonal and cubic phases. For the low-temperature (orthorhombic) phase of bromide and chloride containing structures, local clusters are more likely to form (if their formation is not kinetically hindered). Thus, we conclude that for temperatures at which photovoltaic solar cells usually operate (room temperature and above), it would indeed be possible to synthesize stable mixed compounds with different $Pb:Sn$ stoichiometries for all three halogen groups.

VI. ACKNOWLEDGEMENT

We gratefully acknowledge financial support from the Thüringer Landesgraduiertenschule PhotoGrad and the German Academic Exchange Service (DAAD). We thank Henning Schwanbeck from the computing center of the Technische Universität Ilmenau for quick and professional IT support.

-
- [1] M. M. Lee, J. Teuscher, T. Miyasaka, T. N. Murakami and H. J. Snaith; *Efficient hybrid solar cells based on meso-superstructured organometal halide perovskites.*; Science; **338**(6107):643–647 (2012); ISSN 1095-9203; doi: 10.1126/science.1228604.
- [2] H.-S. Kim, C.-R. Lee, J.-H. Im, K.-B. Lee, T. Moehl,

A. Marchioro, S.-J. Moon, R. Humphry-Baker, J.-H. Yum, J. E. Moser, M. Grätzel and N.-G. Park; *Lead iodide perovskite sensitized all-solid-state submicron thin film mesoscopic solar cell with efficiency exceeding 9%.*; Sci. Rep.; **2**:591 (2012); ISSN 2045-2322; doi:10.1038/srep00591.

- [3] J. H. Noh, S. H. Im, J. H. Heo, T. N. Mandal and S. I. Seok; *Chemical Management for Colorful, Efficient, and Stable Inorganic - Organic Hybrid Nanostructured Solar Cells*; Nano Lett.; **13**(4):1764–1769 (2013).
- [4] M. De Bastiani, V. D’Innocenzo, S. D. Stranks, H. J. Snaith and A. Petrozza; *Role of the crystallization substrate on the photoluminescence properties of organo-lead mixed halides perovskites*; APL Mat.; **2**(8):081509 (2014); ISSN 2166-532X; doi:10.1063/1.4889845.
- [5] T. Baikie, Y. Fang, J. M. Kadro, M. Schreyer, F. Wei, S. G. Mhaisalkar, M. Gratzel and T. J. White; *Synthesis and crystal chemistry of the hybrid perovskite (CH₃NH₃)PbI₃ for solid-state sensitised solar cell applications*; J. Mater. Chem. A; **1**(18):5628 (2013); ISSN 2050-7488; doi:10.1039/c3ta10518k.
- [6] G. Giorgi, J. I. Fujisawa, H. Segawa and K. Yamashita; *Small photocarrier effective masses featuring ambipolar transport in methylammonium lead iodide perovskite: A density functional analysis*; J. Phys. Chem. Lett.; **4**(24):4213–4216 (2013); ISSN 19487185; doi:10.1021/jz4023865.
- [7] M. T. Weller, O. J. Weber, P. F. Henry, M. D. Pumpo and T. C. Hansen; *Complete structure and cation orientation in the perovskite photovoltaic methylammonium lead iodide between 100 and 352 K*; Chem. Comm.; **51**:4180–4183 (2015); ISSN 1359-7345; doi:10.1039/C4CC09944C.
- [8] J.-H. Im, J. Chung, S.-J. Kim and N.-G. Park; *Synthesis, structure, and photovoltaic property of a nanocrystalline 2H perovskite-type novel sensitizer (CH₃CH₂NH₃)PbI₃*; Nanoscale Res. Lett.; **7**(1):353 (2012); ISSN 1556-276X; doi:10.1186/1556-276X-7-353.
- [9] M. Safdari, A. Fischer, B. Xu, L. Kloo and J. M. Gardner; *Structure and function relationships in alkylammonium lead(ii) iodide solar cells*; J. Mater. Chem. A; **3**:9201–9207 (2015); ISSN 2050-7488; doi:10.1039/C4TA06174H.
- [10] I. Borriello, G. Cantele and D. Ninno; *Ab initio investigation of hybrid organic-inorganic perovskites based on tin halides*; Phys. Rev. B; **77**(23):1–9 (2008); ISSN 10980121; doi:10.1103/PhysRevB.77.235214.
- [11] C. C. Stoumpos, C. D. Malliakas and M. G. Kanatzidis; *Semiconducting tin and lead iodide perovskites with organic cations: Phase transitions, high mobilities, and near-infrared photoluminescent properties*; Inorg. Chem.; **52**(15):9019–9038 (2013); ISSN 00201669; doi:10.1021/ic401215x.
- [12] N. Pellet, P. Gao, G. Gregori, T.-Y. Yang, M. K. Nazeeruddin, J. Maier and M. Grätzel; *Mixed-organic-cation perovskite photovoltaics for enhanced solar-light harvesting*; Angew. Chem. Int. Edit.; **53**(12):3151–7 (2014); ISSN 1521-3773; doi:10.1002/anie.201309361.
- [13] G. Giorgi, J.-I. Fujisawa, H. Segawa and K. Yamashita; *Organic-Inorganic Hybrid Lead Iodide Perovskite Featuring Zero Dipole Moment Guanidinium Cations: A Theoretical Analysis*; J. Phys. Chem. C; **119**(9):4694–4701 (2015); ISSN 1932-7447; doi:10.1021/acs.jpcc.5b00051.
- [14] N. D. Marco, H. Zhou, Q. Chen, P. Sun, Z. Liu, L. Meng, E.-P. Yao, Y. Liu, A. Schiffer and Y. Yang; *Guanidinium: A Route to Enhanced Carrier Lifetime and Open-Circuit Voltage in Hybrid Perovskite Solar Cells*; Nano Lett.; **16**(2):1009–1016 (2016); ISSN 1530-6992; doi:10.1021/acs.nanolett.5b04060.
- [15] S. Ryu, J. H. Noh, N. J. Jeon, Y. Chan Kim, W. S. Yang, J. Seo and S. I. Seok; *Voltage output of efficient perovskite solar cells with high open-circuit voltage and fill factor*; Energy. Environ. Sci.; **7**(8):2614 (2014); ISSN 1754-5692; doi:10.1039/C4EE00762J.
- [16] N. J. Jeon, H. G. Lee, Y. C. Kim, J. Seo, J. H. Noh, J. Lee and S. I. Seok; *o-Methoxy substituents in spiro-OMeTAD for efficient inorganic-organic hybrid perovskite solar cells*; J. Am. Chem. Soc.; **136**(22):7837–7840 (2014); ISSN 1520-5126; doi:10.1021/ja502824c.
- [17] J.-W. Lee, D.-J. Seol, A.-N. Cho and N.-G. Park; *High-efficiency perovskite solar cells based on the black polymorph of HC(NH₂)₂PbI₃*; Adv. Mater.; **26**(29):4991–4998 (2014); ISSN 1521-4095; doi:10.1002/adma.201401137.
- [18] D. Bi, P. Gao, R. Scopelliti, E. Oveisi, J. Luo, M. Grätzel, A. Hagfeldt and M. K. Nazeeruddin; *High-Performance Perovskite Solar Cells with Enhanced Environmental Stability Based on Amphiphile-Modified CH₃NH₃PbI₃*; Adv. Mater.; **28**(15):2910–2915 (2016); ISSN 09359648; doi:10.1002/adma.201505255.
- [19] W. S. Yang, J. H. Noh, N. J. Jeon, Y. C. Kim, S. Ryu, J. Seo and S. I. Seok; *High-performance photovoltaic perovskite layers fabricated through intramolecular exchange*; Science; **348**(6240):1234–1237 (2015); ISSN 0036-8075; doi:10.1126/science.aaa9272.
- [20] E. Mosconi, A. Amat, M. K. Nazeeruddin, M. Grätzel and F. De Angelis; *First-principles modeling of mixed halide organometal perovskites for photovoltaic applications*; J. Phys. Chem. C; **117**(27):13902–13913 (2013); ISSN 19327447; doi:10.1021/jp4048659.
- [21] E. T. Hoke, D. J. Slotcavage, E. R. Dohner, A. R. Bowring, H. I. Karunadasa and M. D. McGehee; *Reversible photo-induced trap formation in mixed-halide hybrid perovskites for photovoltaics*; Chem. Sci.; **6**(1):613–617 (2014); ISSN 2041-6520; doi:10.1039/C4SC03141E.
- [22] F. Zheng, H. Takenaka, F. Wang, N. Z. Koocher and A. M. Rappe; *First-Principles Calculation of the Bulk Photovoltaic Effect in CH₃NH₃PbI₃ and CH₃NH₃PbI_{3-x}Cl_x*; J. Phys. Chem. Lett.; **6**(1):31–37 (2015); ISSN 1948-7185; doi:10.1021/jz502109e.
- [23] J. Liu, Y. Shirai, X. Yang, Y. Yue, W. Chen, Y. Wu, A. Islam and L. Han; *High-Quality Mixed-Organic-Cation Perovskites from a Phase-Pure Non-stoichiometric Intermediate (FAI)_{1-x}-PbI₂ for Solar Cells*; Adv. Mater.; **33**(27):4918–4923 (2015); ISSN 1521-4095; doi:10.1002/adma.201501489.
- [24] J. Seo, J. H. Noh and S. I. Seok; *Rational Strategies for Efficient Perovskite Solar Cells*; Accounts Chem. Res.; **49**(3):562–572 (2016); ISSN 1520-4898; doi:10.1021/acs.accounts.5b00444.
- [25] Y. Wang, T. Gould, J. F. Dobson, H. Zhang, H. Yang, X. Yao and H. Zhao; *Density functional theory analysis of structural and electronic properties of orthorhombic perovskite CH₃NH₃PbI₃*; Phys. Chem. Chem. Phys.; **16**(4):1424–1429 (2014); ISSN 1463-9084; doi:10.1039/c3cp54479f.
- [26] F. Hao, C. C. Stoumpos, D. H. Cao, R. P. H. Chang and M. G. Kanatzidis; *Lead-free solid-state organic-inorganic halide perovskite solar cells*; Nat. Photonics; **8**(6):489–494 (2014); ISSN 1749-4885; doi:10.1038/nphoton.2014.82.
- [27] N. K. Noel, S. D. Stranks, A. Abate, C. Wehrenfennig, S. Guarnera, A.-A. Haghighirad, A. Sadhanala, G. E. Eperon, S. K. Pathak, M. B. Johnston, A. Petrozza, L. M. Herz and H. J. Snaith; *Lead-Free Organic-Inorganic Tin Halide Perovskites for Photovoltaic Appli-*

- cations; Energy Environ. Sci.; **7**:3061–3068 (2014); ISSN 1754-5692; doi:10.1039/C4EE01076K.
- [28] C. Bernal and K. Yang; *First-Principles Hybrid Functional Study of the Organic-Inorganic Perovskites $\text{CH}_3\text{NH}_3\text{SnBr}_3$ and $\text{CH}_3\text{NH}_3\text{SnI}_3$* ; J. Phys. Chem. C; **118**(42):24383–24388 (2014).
- [29] F. Hao, C. C. Stoumpos, R. P. H. Chang and M. G. Kanatzidis; *Anomalous band gap behavior in mixed Sn and Pb perovskites enables broadening of absorption spectrum in solar cells*; J. Am. Chem. Soc.; **136**(22):8094–8099 (2014); doi:10.1021/ja5033259.
- [30] F. Zuo, S. T. Williams, P. W. Liang, C. C. Chueh, C. Y. Liao and A. K. Y. Jen; *Binary-metal perovskites toward high-performance planar-heterojunction hybrid solar cells*; Adv. Mater.; **26**(37):6454–6460 (2014); ISSN 09359648; doi:10.1002/adma.201401641.
- [31] Y. Ogomi, A. Morita, S. Tsukamoto, T. Saitho, N. Fujikawa, Q. Shen, T. Toyoda, K. Yoshino, S. S. Pandey and S. Hayase; *$\text{CH}_3\text{NH}_3\text{Sn}_x\text{Pb}_{x-1}\text{I}_3$ Perovskite Solar Cells Covering up to 1060 nm*; J. Phys. Chem. Lett.; **5**(6):1004–1011 (2014).
- [32] E. Mosconi, P. Umari and F. De Angelis; *Electronic and optical properties of mixed Sn–Pb organohalide perovskites: a first principles investigation*; J. Mater. Chem. A; **3**:9208–9215 (2015); ISSN 2050-7488; doi:10.1039/C4TA06230B.
- [33] G. Kresse and J. Hafner; *Ab initio molecular dynamics for liquid metals*; Phys. Rev. B; **47**(1):558–561 (1993); doi:10.1103/PhysRevB.47.558.
- [34] G. Kresse and J. Furthmüller; *Efficient iterative schemes for ab initio total-energy calculations using a plane-wave basis set*; Phys. Rev. B; **54**(16):11169–11186 (1996); doi:10.1103/PhysRevB.54.11169.
- [35] P. E. Blochl; *Projector augmented-wave method*; Phys. Rev. B; **50**(24):17953–17979 (1994); doi:10.1103/PhysRevB.50.17953.
- [36] G. Kresse and D. Joubert; *From ultrasoft pseudopotentials to the projector augmented-wave method*; Phys. Rev. B; **59**(3):1758–1775 (1999); doi:10.1103/PhysRevB.59.1758.
- [37] J. P. Perdew, K. Burke and M. Ernzerhof; *Generalized Gradient Approximation Made Simple*; Phys. Rev. Lett.; **77**(18):3865–3868 (1996); ISSN 0031-9007; doi:10.1103/PhysRevLett.77.3865.
- [38] P. Haasen; *Physical Metallurgy*; Cambridge University Press; 3 edn. (1996); ISBN 0521550920.
- [39] P. J. Flory and W. R. Krigbaum; *Thermodynamics of High Polymer Solutions*; Annu. Rev. Phys. Chem.; **2**(1):383–402 (1951); ISSN 0066-426X; doi:10.1146/annurev.pc.02.100151.002123.
- [40] M. L. Huggins; *Thermodynamic properties of solutions of high polymers: The empirical constant in the activity equation*; Ann. N. Y. Acad. Sci.; **44**(4):431–443 (1943); ISSN 00778923; doi:10.1111/j.1749-6632.1943.tb52763.x.
- [41] M. Tricker and J. Donaldson; *Comments on the structure, bonding and ^{119}Sn Mössbauer parameters of tin(II) derivatives of the type MSnX_3* ; Inorg. Chim. Acta.; **31**(C):L445–L446 (1978); ISSN 00201693; doi:10.1016/S0020-1693(00)94957-0.
- [42] A. Poglitsch and D. Weber; *Dynamic disorder in methylammoniumtrihalogenoplumbates (II) observed by millimeter-wave spectroscopy*; J. Chem. Phys.; **87**(11):6373 (1987); ISSN 00219606; doi:10.1063/1.453467.
- [43] J. M. Frost, K. T. Butler and A. Walsh; *Molecular ferroelectric contributions to anomalous hysteresis in hybrid perovskite solar cells*; APL Mat.; **2**(8):081506 (2014); ISSN 2166-532X; doi:10.1063/1.4890246.
- [44] F. D. Murnaghan; *The Compressibility of Media under Extreme Pressures*; Proc. Natl. Acad. Sci. USA; **30**(9):244–247 (1944); ISSN 0027-8424; doi:10.1073/pnas.30.9.244.
- [45] P. M. Woodward; *Octahedral Tilting in Perovskites. I. Geometrical Considerations*; Acta Crystallogr. B; **53**(1):32–43 (1997); ISSN 01087681; doi:10.1107/S0108768196010713.
- [46] P. Garcia-Fernandez, J. Aramburu, M. Barriuso and M. Moreno; *Key Role of Covalent Bonding in Octahedral Tilting in Perovskites*; J. Phys. Chem. Lett.; **1**(3):647–651 (2010); ISSN 1948-7185; doi:10.1021/jz900399m.
- [47] O. Knop, R. E. Wasylshen, M. A. White, T. S. Cameron and M. J. M. V. Oort; *Alkylammonium lead halides. Part 2. $\text{CH}_3\text{NH}_3\text{PbX}_3$ ($X = \text{Cl}, \text{Br}, \text{I}$) perovskites: cuboctahedral halide cages with isotropic cation reorientation*; Can. J. Chem.; **68**(3):412–422 (1990); ISSN 0008-4042; doi:10.1139/v90-063.
- [48] H. Mashiyama; *Disordered Cubic Perovskite Structure of $\text{CH}_3\text{NH}_3\text{PbX}_3$ ($X = \text{Cl}, \text{Br}, \text{I}$)*; J. Korean Phys. Soc.; **32**:S156–S158 (1998); ISSN 03744884.
- [49] Y. Takahashi, R. Obara, Z.-Z. Lin, Y. Takahashi, T. Naito, T. Inabe, S. Ishibashi and K. Terakura; *Charge-transport in tin-iodide perovskite $\text{CH}_3\text{NH}_3\text{SnI}_3$: origin of high conductivity*; Dalton Trans.; **40**(20):5563–5568 (2011); ISSN 1477-9226; doi:10.1039/c0dt01601b.
- [50] D. Weber; *$\text{CH}_3\text{NH}_3\text{SnBr}_x\text{I}_{3-x}$ ($x=0-3$), ein Sn(II)-System mit kubischer Perowskitstruktur*; Z. Naturforsch. B; **33**(8):862–865 (1978).
- [51] N. Onoda-Yamamuro, T. Matsuo and H. Suga; *Thermal, electric, and dielectric properties of $\text{CH}_3\text{NH}_3\text{SnBr}_3$ at low temperatures*; J. Chem. Thermodyn.; **23**(39):987–999 (1991).